

Vol. 14 • No. 28 • July 12 • 2018

[www.small-journal.com](http://www.small-journal.com)

# NANO • MICRO small



WILEY-VCH

# A Fully Biodegradable Battery for Self-Powered Transient Implants

Xueying Huang, Dan Wang, Zhangyi Yuan, Wensheng Xie, Yixin Wu, Rongfeng Li, Yu Zhao, Deng Luo, Liang Cen, Binbin Chen, Hui Wu, Hangxun Xu, Xing Sheng, Milin Zhang, Lingyun Zhao, and Lan Yin\*

**Biodegradable transient devices represent an emerging type of electronics that could play an essential role in medical therapeutic/diagnostic processes, such as wound healing and tissue regeneration. The associated biodegradable power sources, however, remain as a major challenge toward future clinical applications, as the demonstrated electrical stimulation and sensing functions are limited by wired external power or wireless energy harvesters via near-field coupling. Here, materials' strategies and fabrication schemes that enable a high-performance fully biodegradable magnesium–molybdenum trioxide battery as an alternative approach for an in vivo on-board power supply are reported. The battery can deliver a stable high output voltage as well as prolonged lifetime that could satisfy requirements of representative implantable electronics. The battery is fully biodegradable and demonstrates desirable biocompatibility. The battery system provides a promising solution to advanced energy harvesters for self-powered transient bioresorbable implants as well as eco-friendly electronics.**

Biodegradable electronics is an emerging type of technology whose main characteristic is the capability of degradation in physiological or environmental aqueous solutions at controlled rates, and is referred to as “transient electronics.”<sup>[1–5]</sup> Such

X. Huang, D. Wang, W. Xie, Y. Wu, Dr. R. Li, L. Cen, B. Chen, Prof. H. Wu, Prof. L. Zhao, Prof. L. Yin

School of Materials Science and Engineering  
The Key Laboratory of Advanced Materials of Ministry of Education  
State Key Laboratory of New Ceramics and Fine Processing  
Tsinghua University  
Beijing 100084, P. R. China  
E-mail: lanyin@tsinghua.edu.cn

Z. Yuan, Y. Zhao, D. Luo, Prof. X. Sheng, Prof. M. Zhang  
Department of Electronic Engineering  
Tsinghua University  
Beijing 100084, P. R. China

Y. Wu  
Department of Materials Science and Engineering  
Northwestern University  
Evanston, IL 60208, USA

Prof. H. Xu  
Hefei National Laboratory for Physical Sciences at the Microscale  
Department of Polymer Science and Engineering  
University of Science and Technology of China  
Hefei, Anhui 230026, P. R. China

 The ORCID identification number(s) for the author(s) of this article can be found under <https://doi.org/10.1002/sml.201800994>.

DOI: 10.1002/sml.201800994

electronic platforms can serve as temporary implants to perform sensing and stimulation functions that can influence critical biological processes such as wound healing, tissue regeneration, and brain activity.<sup>[6,7]</sup> The biodegradability of the electronic system eliminates a second surgery for device retrieval and, therefore, could reduce potential risks and chronic inflammation caused by permanent devices, as well as associated hospital costs. Other potential applications include eco-friendly devices that alleviate issues (e.g., landfill space and hazardous components) associated with electronic-waste (e-waste)<sup>[8]</sup> and data-secure hardware systems that prevent unauthorized access to personal or security information.<sup>[9–11]</sup> Translation of these technologies could potentially provide vital tools that are beneficial for human health-care and the environment.

Although biodegradable materials (semiconductors, metals, dielectrics, etc.) have been extensively studied and a variety of transient devices have been achieved,<sup>[1–5]</sup> the biodegradable power source remains as one major challenge toward future clinical applications. Current demonstrations of biodegradable electronics are limited by the use of wired external power or wireless energy harvesters via near-field coupling,<sup>[6,7,12]</sup> where the device position and orientation could be significantly constrained. Dissolvable piezoelectric energy harvesters,<sup>[13]</sup> supercapacitors,<sup>[14,15]</sup> and solar cells<sup>[16]</sup> have been proposed as possible power tools. However, they either suffer from relatively low energy density or location limitations. The biodegradable battery represents an alternative promising on-board power solution due to its capability of independent deployment and attainable high energy density. With a robust biodegradable battery, self-powered diagnostic and therapeutic biodegradable implants could be achieved, enabling in vivo sensing and stimulation over longer time frames relevant to clinical standards and can be fully resorbable afterward, which would otherwise be impossible with existing technologies. Biodegradable batteries are therefore of particular interest for in vivo applications, but so far only limited progress has been accomplished.

Conventional batteries usually consist of carbon, relatively inert metals (e.g., aluminum and stainless steel), nondegradable polymer (e.g., polypropylene), oxides, and hazardous electrolyte, which are either not degradable or could be harmful to human health.<sup>[17]</sup> By introducing dissolvable metals and

oxides with biocompatible dissolution products,<sup>[18]</sup> and biodegradable polymers that are capable of hydrolysis in aqueous solutions,<sup>[19]</sup> fully encapsulated biodegradable battery systems are possible. Currently available biobatteries are mostly primary cells utilizing metallic electrodes, e.g., magnesium (Mg) or zinc (Zn) galvanic cells, with the advantage of excellent biocompatibility and high energy density. Reported systems include fully biodegradable Mg–Mo battery systems that can power a light-emitting diode (LED) and a wireless radio circuit,<sup>[20]</sup> and partially degradable batteries such as Zn–Cu cells for prolonged in vivo temperature sensing and wireless communication,<sup>[21]</sup> Mg–CuCl<sub>2</sub> cell for integrated-circuit microsensors,<sup>[22]</sup> microfabricated Mg–Fe batteries,<sup>[23,24]</sup> and Mg–air and Mg alloy (AZ31)–air batteries based on silk fibroin or gel electrolyte.<sup>[25–27]</sup> Alternative strategies with nonmetallic electrode materials have been proposed, such as edible sodium-ion batteries based on melanins<sup>[28]</sup> or activated carbon<sup>[29]</sup> and sugar-based enzymatic fuel cells.<sup>[30,31]</sup> Eco-friendly battery systems targeting nonbiological applications have also been presented, including transient lithium-ion batteries through chemical reactions<sup>[32]</sup> or chemical/mechanical disintegration<sup>[33]</sup> and primary flow battery using organic quinone redox species.<sup>[34]</sup> The major challenges of these systems are either containing nondegradable or nonbiocompatible battery components resulting in unnecessary materials retention that could cause adverse effects to the human body and the environment, or battery characteristics (e.g., voltage, power, capacity, or lifetime) that could fall beyond practical applications.

Here, we propose new materials' strategies and fabrication schemes that enable a high-performance fully biodegradable primary magnesium–molybdenum trioxide (Mg–MoO<sub>3</sub>) battery system. Mg serves as the anode material and possesses high theoretical energy density (2200 mAh g<sup>-1</sup>) with excellent biocompatibility (daily allowance ≈ 300 mg d<sup>-1</sup>). Although being extensively investigated as electrodes for lithium-ion batteries, MoO<sub>3</sub> has not been explored for biobatteries.<sup>[35]</sup> Together with its solubility in aqueous solution (≈1 g L<sup>-1</sup>) and desirable biocompatibility at controlled level,<sup>[36,37]</sup> MoO<sub>3</sub> is expected to be a suitable cathode material for biodegradable batteries. Based on the electrode materials, a high stable output voltage up to 1.6 V of a single cell battery is achieved, which is equivalent to that of a commercial alkaline battery. Introducing alginate hydrogel electrolyte and polyanhydride/poly(lactide-co-glycolide) (PLGA) coating can significantly prolong the lifetime of the battery system to be ≈13 d. Energy provided by the single Mg–MoO<sub>3</sub> cell is sufficient to power a red LED, a calculator, and the amplifier of an electrocardiogram (ECG) signal detector. The voltage and power provided by the battery could satisfy most of the ultralow-power implantable devices as well as maintain robust functions, as the required voltage and power are typically in the range of ≈0.5–1.6 V<sup>[38,39]</sup> and ≈10–1000 μW,<sup>[40]</sup> respectively, thanks to the advanced design techniques and technology developments of complementary metal–oxide–semiconductor (CMOS) devices. The battery is fully degradable both in vitro and in vivo, and desirable biocompatibility of degradation products has been observed. The battery system could potentially provide a promising energy solution to unique self-powered biodegradable electronic implants that can play an essential role in advanced diagnosis and treatment for major diseases.

The schematic structure of the biodegradable Mg–MoO<sub>3</sub> battery is given in **Figure 1A**. Mg foil serves as the anode and sodium alginate (ALG-Na) hydrogel with phosphates works as the electrolyte. The cathode part consists of an active MoO<sub>3</sub> layer on top of a Mo foil. The MoO<sub>3</sub> film is achieved by mixing MoO<sub>3</sub> powders and a biodegradable polymer (e.g., PLGA) as the binder. Microstructure investigation reveals a 3D network structure within the MoO<sub>3</sub> film, as the scanning electron microscopy (SEM) images in **Figure 1B,C**. An enlarged view of the MoO<sub>3</sub> film appears in **Figure 1D**, and it shows the connections of MoO<sub>3</sub> particles by PLGA binders. As the PLGA binder is permeable to the water content in the electrolyte, the network allows a 3D porous structure for chemical reactions that can increase the effective surface area and promote battery performance.

The discharge behavior of a single Mg–MoO<sub>3</sub> cell with different MoO<sub>3</sub> film thicknesses is given in **Figure 1E**, at a discharge current density of 0.025 mA cm<sup>-2</sup>. A stable voltage up to 1.6 V is achieved and can last for more than 48 h in the battery with thicker MoO<sub>3</sub> film (350 μm). Thinner films result in a faster consumption of MoO<sub>3</sub> materials and therefore a quicker decline in the output voltage. As shown in **Figure 1F**, with the MoO<sub>3</sub> film of 200 μm, the cell is capable of providing a voltage exceeding 1.45 V for over 50 h, followed by a transition to an output voltage of ≈0.6 V comparable to that of a Mg–Mo battery,<sup>[20]</sup> which lasts for ≈250 h. The results suggest that the decline of the battery voltage comes from the consumption of MoO<sub>3</sub>. Compared to the cell using an aqueous phosphate buffered saline (PBS) electrolyte, introducing the hydrogel electrolyte can significantly prolong the total lifetime of the battery (**Figure 1F**, 300 vs 60 h), due to the restricted side reactions, i.e., corrosion of Mg and dissolution of MoO<sub>3</sub>. The discharge behavior with different current density is also investigated, and the results appear in **Figure 1G**. The high voltage of ≈1.5 V can be sustained for a current density up to 0.15 mA cm<sup>-2</sup>, and it drops significantly when the current density exceeds 0.3 mA cm<sup>-2</sup>. The corresponding voltage and power are summarized in **Figure 1H**. The voltage is obtained by averaging the data from the first five hours. The current density at 0.3 mA cm<sup>-2</sup> achieves the highest power of 0.27 mW cm<sup>-2</sup>.

A comparison with previously reported biobattery regarding the output voltage and specific capacity at similar discharge current densities is given in **1I** and in **Table S1** (Supporting Information). As is shown, the output voltage of most reported cells is in the range of 0.2–0.9 V, and multicell connections or voltage-promoting circuits are therefore necessary for practical applications. Nondissolvable components are also present in most of these systems, which could result in unnecessary materials retention and cause potential adverse effects. Moreover, the capacity and lifetime of the batteries depend on the type and the amount of the active material, as well as the battery configurations. The lifetime of most reported biobatteries shown in **Figure 1I** and **Table S1** (Supporting Information) are in the range of a few minutes to a few days, e.g., AZ31–air (≈0.9 V) and Mg–Fe (≈0.8 V) cells have been reported to be functional for 2.5 and 4 d, respectively.<sup>[24,27]</sup> However, broader operation time frames are probably more desirable as sensing and stimulation functions of therapeutic systems could take up to a few weeks. In all, Mg–MoO<sub>3</sub> battery reported in the current work demonstrates the advantages of offering elevated stable voltage

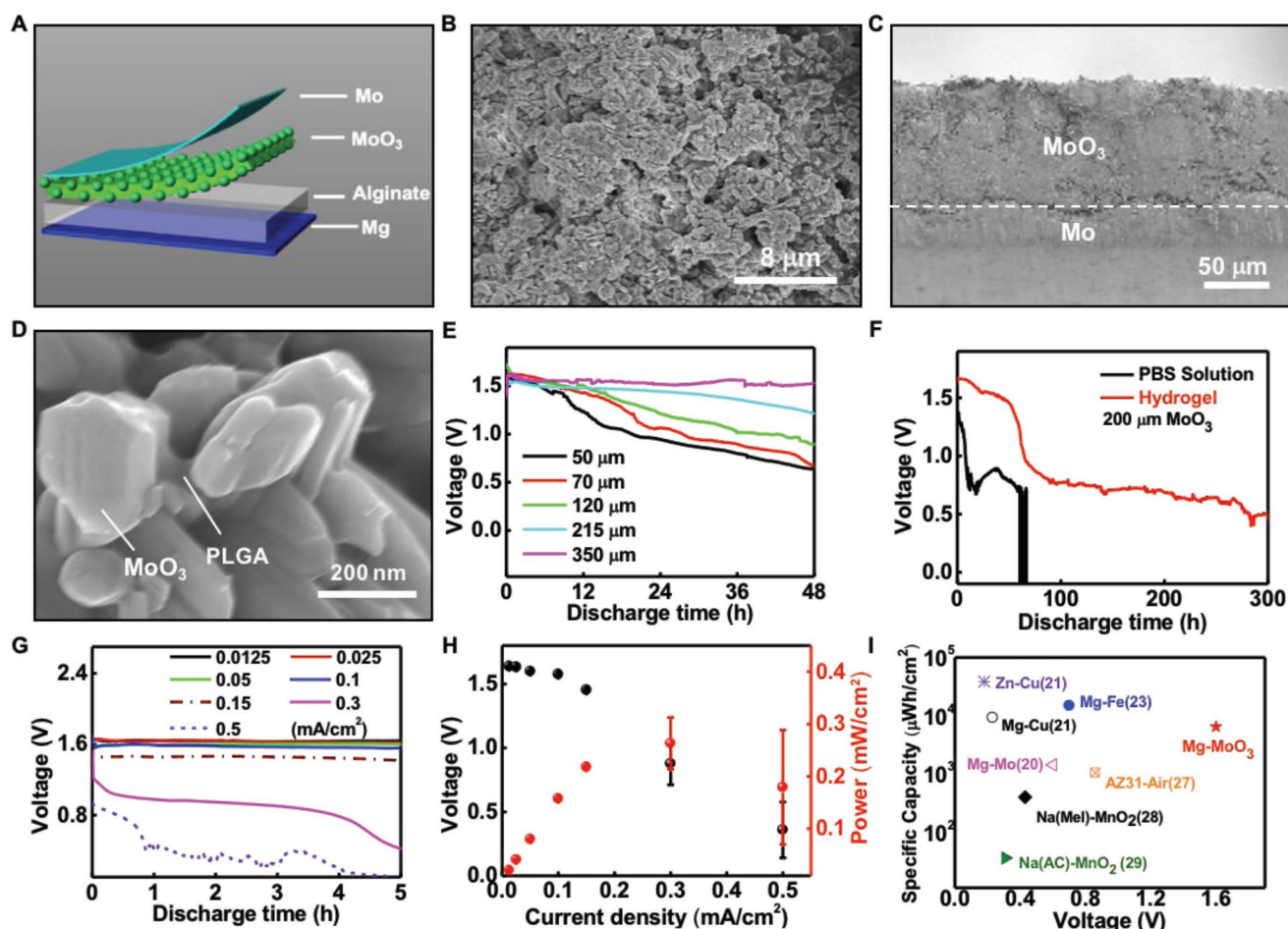


**Figure 1.** Materials, structure, and discharge behavior of the biodegradable battery. A) The schematic illustration of the battery structure. B) The SEM image of the cathode  $\text{MoO}_3/\text{PLGA}$  layer. C) Cross-sectional view of the cathode layer. D) Enlarged view of the cathode layer. E) Discharge behavior with different  $\text{MoO}_3$  thicknesses (discharge current density:  $25 \mu\text{A cm}^{-2}$ ). F) Discharge performance with hydrogel and phosphate buffered saline electrolytes (discharge current density:  $25 \mu\text{A cm}^{-2}$ ). G) Discharge behavior with different discharge current densities. H) Summary of battery voltage and power as a function of discharge current densities. I) Specific capacity versus voltage of reported biobatteries.

(up to 1.6 V), prolonged operational lifetime ( $\approx 1.5$  V for 50 h and  $\approx 0.6$  V for 250 h,  $\approx 13$  d in total), and high energy capacity ( $6.5 \text{ mWh cm}^{-2}$ ) as well as full biodegradability (will be shown later) that could satisfy the requirements of a broader range of implantable devices.

Electrochemical evaluation has been performed to study the electrode characteristics of the Mg– $\text{MoO}_3$  battery system. The potential between Mg and  $\text{MoO}_3$  electrodes and the potential of the individual electrodes with respect to saturated Ag/AgCl reference electrode are investigated via a galvanodynamic scan with current densities ranging from 0 to  $1 \text{ mA cm}^{-2}$  using hydrogel electrolyte (Figure 2A). The potential of Mg with respect to Ag/AgCl remains relatively stable around  $-1.6$  V throughout the scanning range, which is comparable to the reported value.<sup>[20]</sup> The potential of the  $\text{MoO}_3$  electrode decreases with increasing current density and exhibits a two-stage behavior. The electrochemical impedance spectroscopy (EIS) measurements of the electrode and the battery are given in Figure 2B. The impedance at the cathode site ( $\text{MoO}_3$ ) is higher than that of the anode site (Mg), and the resistance of the alginate gel electrolyte is shown to be  $\approx 20 \Omega$ . To evaluate

the effectiveness of the 3D network structure based on the powder/PLGA electrode, performance of the battery using Mo foil ( $30 \mu\text{m}$ ), Mo paste (powder/PLGA,  $150 \mu\text{m}$ ),  $\text{MoO}_3$  thin film ( $1 \mu\text{m}$ , magnetron sputtering), and  $\text{MoO}_3$  paste (powder/PLGA,  $150 \mu\text{m}$ ) as the cathode materials is investigated and the results appear in Figure 2C. The usage of the Mo paste results in an increase of 30% of the output voltage compared to that of the Mo foil, probably due to the increase in the active surface area of the 3D network structure. On the other hand, the  $\text{MoO}_3$  paste cathode achieves an increase of 1 V compared to that of the  $\text{MoO}_3$  thin film, probably due to the increase in effective surface area as well as the conductivity of the  $\text{MoO}_3$  layer. The results suggest that the simple method of preparing  $\text{MoO}_3/\text{PLGA}$  layer can successfully promote the battery performance. Cyclic voltammetry (CV) is used to study the  $\text{MoO}_3$  electrode behavior, and the results are shown in Figure S1A–C in the Supporting Information. The results indicate the possible reduction of Mo(VI) and intercalation of Mg ions (dissolution products from Mg anode) and Ca ions (the cross-linker for hydrogel) into the oxide matrix during the discharge process, which is supported by the energy dispersive

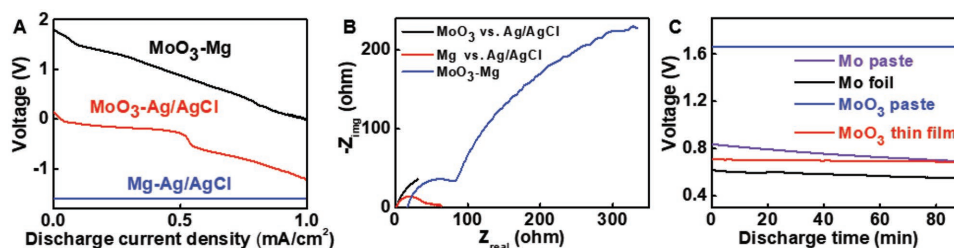


**Figure 2.** Electrode characteristics of the battery. A) Galvanodynamic scanning of full cell and individual electrodes (scanning rate:  $2 \mu\text{A s}^{-1}$ ). B) Electrochemical impedance spectra of full cell and individual electrodes. C) Discharge behavior of batteries with different cathode materials.

spectrometer (EDS) results given in Figure S1D,E in the Supporting Information.

A representative single cell Mg–MoO<sub>3</sub> battery encapsulated with biodegradable polyanhydride and PLGA layers is given in Figure 3A. Due to the achieved high output voltage, the power of a single cell is sufficient to light up a red-light LED (threshold voltage  $\approx 1.5$  V). As shown in Figure 3B and Figure S2A (Supporting Information), the powered LED can maintain its function in phosphate buffered saline at room temperature for up to 16 h, indicating the potential usage in aqueous environments of the current battery configuration. The light intensity of the LED does not show a distinct difference over time until it goes off after 16 h.

Figure 3C illustrates a general calculator, consisting of user input buttons and liquid crystal display (LCD), powered up by the proposed single cell Mg–MoO<sub>3</sub> battery. The battery can also drive the amplifier of a low power ECG signal detector. The block diagram of the ECG test setup appears in Figure S2B (Supporting Information) and a photo of the measurement system is given in Figure S2C (Supporting Information). The designed amplifier of the detector can work under a supply voltage of 1.3 V. The measured output signal is shown in

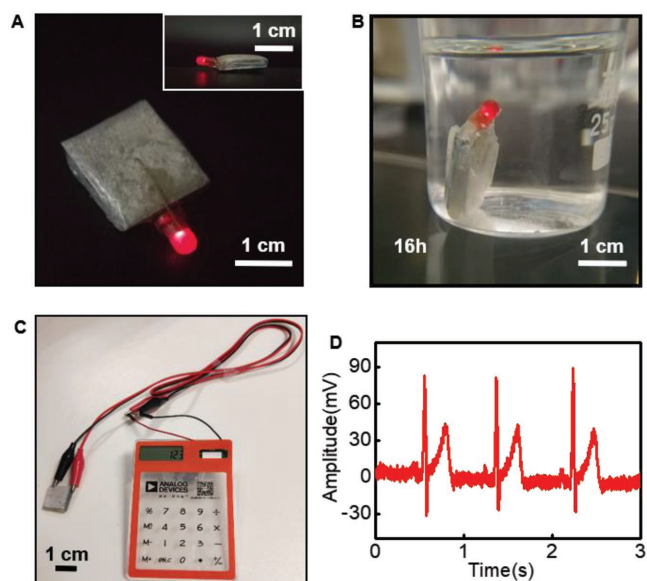


**Figure 3.** A) A red LED powered by the battery, with a side view in the inset. B) The battery drives the LED in phosphate buffered saline for over 16 h. C) A calculator powered by the battery. D) Measured ECG signal with the amplifier of the detector powered by the biodegradable battery.

Figure 3D, which is comparable to that using a 1.8 V nontransient external power source (Figure S2D, Supporting Information). The experimental results demonstrate that the battery is sufficient to power up typical functional circuits. The driving capability provided by the degradable battery is promising to satisfy ultralow-power, ultralow-voltage devices designed for, i.e., biomedical implants and/or Internet of Things (IoT) applications.

Figure 4A illustrates the optical images of various stages of the dissolution process of the biodegradable battery in phosphate buffered saline. The polyanhydride and PLGA encapsulation degrade first, followed by the disintegration of the battery. The dissolution of Mg, sodium alginate hydrogel, MoO<sub>3</sub>/PLGA layer, and Mo takes place at the same time, and most materials (e.g., Mg, alginate, and MoO<sub>3</sub>/PLGA) completely dissolve within 9 d except Mo which needs another 10 d to entirely disappear at elevated temperature (85 °C). Dissolution rates of Mg and Mo foils have been reported to be  $\approx 1\text{--}10 \mu\text{m d}^{-1}$  and  $0.02 \mu\text{m d}^{-1}$  in simulated biofluids (pH 7.4, 37 °C), respectively.<sup>[18,41]</sup> The degradation rates of biopolymers depend on their specific chemistry, molecular weight, terminal groups, etc.; for example, partially oxidized alginate losses 70% of molecular weight within 5 d, PLGA (65:35) losses 50% of mass after  $\approx 18$  d,<sup>[42,43]</sup> while polyanhydride fully degrades within 48 h in moisturized environments.<sup>[11,20,44]</sup> Although MoO<sub>3</sub> is expected to dissolve quickly in aqueous solutions due to its high solubility ( $\approx 1 \text{ g L}^{-1}$ ), its degradation rate is modulated by the PLGA binder and encapsulation layers. The observed degradation rates of the battery materials (e.g., metallic films, alginate, and polyanhydride) are comparable with the reported results in the literature, while PLGA dissolves faster probably due to the thin-film formats of the layer ( $< 20 \mu\text{m}$ ).

To evaluate the biocompatibility of the cathode materials of the battery, the Cell Count Kit-8 (CCK-8) assay and Calcein-AM/propidium Iodide (PI) staining are employed to investigate the cytotoxicity of MoO<sub>3</sub> paste electrode encapsulated by a PLGA layer. After co-incubation of L-929 mouse fibroblast cells with the MoO<sub>3</sub>/PLGA films for different times, cell viability and fluorescent images of the cells were shown in Figure 4B and Figure 4C, respectively. Both the viability data and fluorescent images indicate that MoO<sub>3</sub> demonstrates ideal biocompatibility, as no noticeable difference in cell viability is observed of PLGA samples with and without the MoO<sub>3</sub> component. Moreover, the existence of MoO<sub>3</sub> is also found to increase the growth ability of the L-929 cells, consistent with the results reported in a previous work that the addition of 7 mol% MoO<sub>3</sub> in the glass sample presents high biocompatibility with HaCaT cells.<sup>[37]</sup> The cell

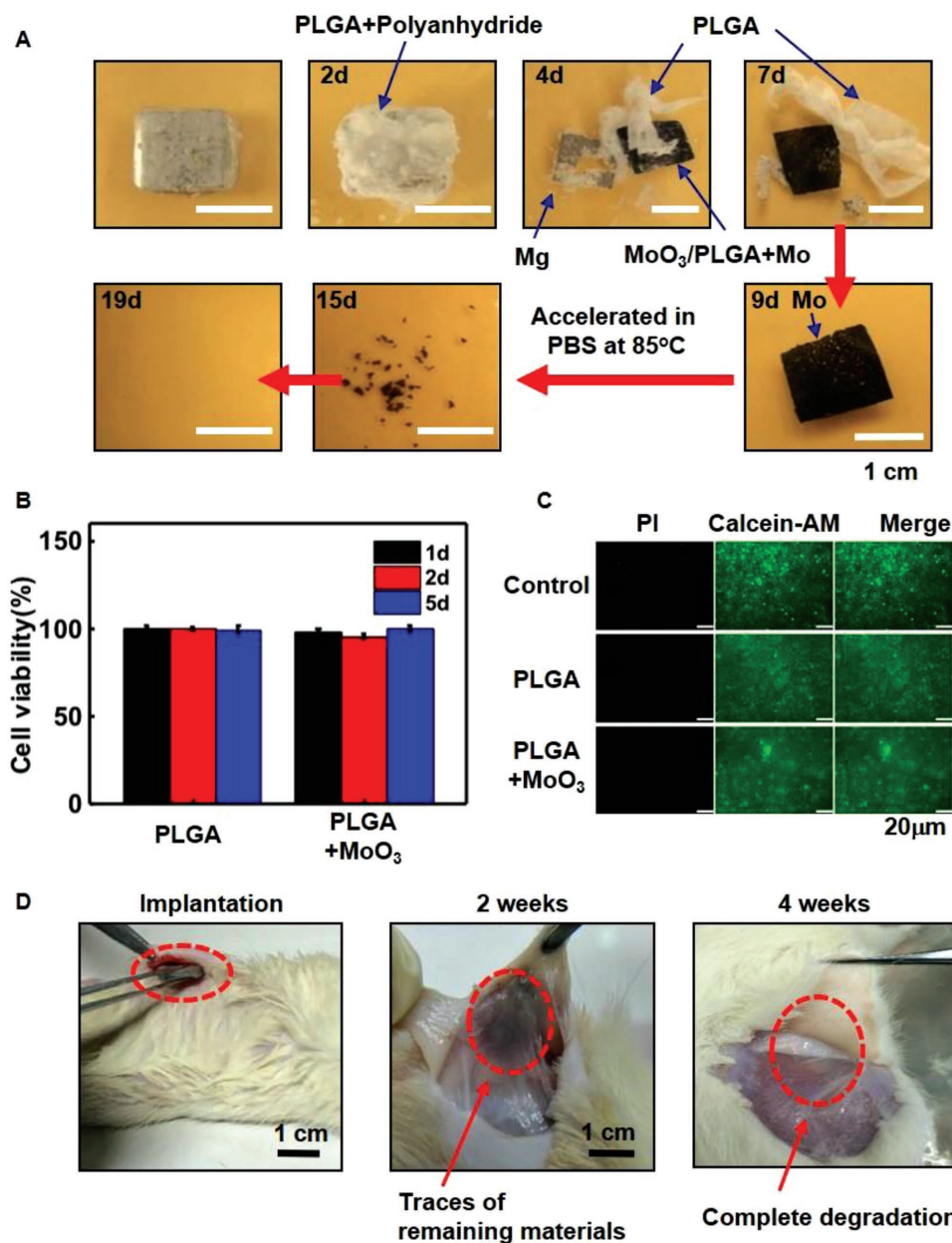


**Figure 4.** Degradation and biocompatibility evaluation of the battery materials. A) Optical images at various stages of dissolution of the battery in phosphate buffered saline. B) Cell viability of MoO<sub>3</sub>/PLGA and PLGA films over 1, 2, and 5 d calculated as the fraction of total living cells. C) Fluorescent images showing the cell viability, with Green (Calcein-AM)/red (PI) represents live/dead L-929 cells, respectively. D) In vivo degradation evaluation of the battery in the subcutaneous area of SD rats: (left) battery implantation, (center) 2 weeks after implantation, and (right) 4 weeks after implantation suggesting complete degradation of the whole battery.

culture medium is refreshed every day, and the medium at 1, 3, and 5 d is sampled to evaluate the Mo concentration through inductively coupled plasma optical emission spectrometry (ICP-OES). The results are summarized in Table S2 (Supporting Information). The release rate of Mo is mainly controlled by the encapsulation layer (e.g., PLGA). As dissolution proceeds, the encapsulation polymer swells and degrades, similar to the process shown in Figure 4A, and therefore a significant increase in Mo release rate is observed around day 3. The concentration of Mo then drops after all the MoO<sub>3</sub> dissolves and the solution

is refreshed. The results indicate that by engineering the chemistry and thickness of the encapsulation layers, the release rate of Mo can be controlled within a desirable level, and a proper level of molybdenum (up to  $\approx 370 \mu\text{g mL}^{-1}$ ) is compatible with cell growth in the current experiments.

In vivo experiments performed subcutaneously on the Sprague–Dawley (SD) rat model demonstrates full degradability of the entire battery. A biodegradable battery ( $\approx 1.2 \times 1.2 \times 0.4 \text{ cm}$ ) with a shape similar to the undissolved cell shown in Figure 4A was implanted in the subdermal region of

the rats (Figure 4D). Traces of battery components are observed in the subdermal region after 2 weeks, followed by the complete disappearance after implantation of 4 weeks, as shown in Figure 4D. The *in vivo* degradation rate is faster compared to that of the *in vitro* process, probably due to the difference in the aqueous environments and circulation conditions. The hematoxylin–eosin (HE) staining of skin tissues and different organs indicates no overt cell reaction to the battery and its dissolution products (Figure S3, Supporting Information). Overall, both *in vitro* and *in vivo* experiments show desirable biocompatibility and demonstrate the feasibility of *in vivo* application of the fully degradable battery.

The materials strategies and fabrication schemes proposed in this work enable a high-performance fully biodegradation battery system. Introducing MoO<sub>3</sub> to the cathode materials achieves an increase in the output voltage by a factor of 3 compared to that of the Mg–Mo battery systems,<sup>[20]</sup> and is higher than most of the biobatteries reported in the literature. The increase in the output voltage is attributed to the reduction of Mo(VI) at the cathode site as well as the 3D network structure. The reaction takes place at the Mg anode site is believed to be



with a side reaction with the aqueous electrolyte



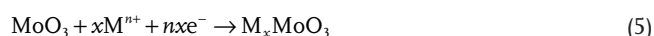
Although the theoretical potential of Mg/Mg<sup>2+</sup> with respect to Ag/AgCl is –2.69 V, the measured potential is ≈–1.6 V, probably due to the coating of the dissolution product Mg(OH)<sub>2</sub> on the Mg surface, which aligns well with the reported values in the literature.<sup>[20]</sup> As for the cathode site, the reaction of a metallic electrode is supposed to be either hydrogen evolution or oxygen reduction.



or



whereas for the MoO<sub>3</sub> cathode, in the analogy to lithium-ion battery, the reaction is speculated to be the reduction of Mo(IV)<sup>[35]</sup>



The presence of Mg and Ca ions could intercalate and affect the possible reactions at the cathode sites, as the CV and SEM–EDS results shown in Figure S1 (Supporting Information), which are similar to the intercalation behavior of Mg ion into the MoO<sub>3</sub> thin film in the Mg/V<sub>2</sub>O<sub>5</sub> and Mg/MoO<sub>3</sub> systems.<sup>[45]</sup> The cathode potential is measured to be 0.1 V, which promotes the output voltage compared to that of the Mg–Mo battery. The active component MoO<sub>3</sub> at the cathode site also gradually dissolves as the battery discharges, which is considered as another side reaction. As the MoO<sub>3</sub> material consumes, the battery performance transits to the behavior of a Mg–Mo battery.

The simple method of preparing the cathode materials by mixing MoO<sub>3</sub> powder and PLGA results in a 3D MoO<sub>3</sub> network where the PLGA constituent is permeable to the aqueous

component in the electrolyte. The structure therefore effectively promotes the active surface area, resulting in an elevated output voltage and current capability. As shown in Figure 1G, the battery can maintain a high voltage (≈1.5 V) for a current density up to 0.15 mA cm<sup>–2</sup>. Hydrogel electrolyte instead of an aqueous electrolyte significantly prolongs the lifetime of the biodegradable battery by five times, as it helps suppress the side reaction of both Mg and MoO<sub>3</sub>. A total capacity of 6.5 mWh cm<sup>–2</sup> and a lifetime ≈13 d are achieved, which rank at the top range of the reported systems as illustrated in Figure 1I. As the capacity and lifetime of the biodegradable battery are governed by the amount of active materials and their degradation rates, controlling the thickness and chemistry of Mg-based anode, MoO<sub>3</sub> layer, hydrogel electrolyte, and the encapsulation layer, a tunable performance of the battery can be realized to address the requirements of various applications.

The single-cell Mg–MoO<sub>3</sub> battery demonstrates the capability to power a red LED, a calculator, and the amplifier of an ECG signal detector. Given the high stable voltage (up to 1.6 V), current capability (12.5–150 μA cm<sup>–2</sup>), and capacity (6.5 mWh cm<sup>–2</sup>) provided, the battery is promising to satisfy the voltage, current, and power requirements of most representative ultralow-power devices designed for implantable applications, e.g., ≈10–1000 μW for pacemaker, cardiac defibrillator, neural stimulator, and drug pump;<sup>[40]</sup> 1–1.6 V for neural recording system and integrated neural amplifiers.<sup>[39]</sup> The elevated output voltage compared to reported battery systems ensures robust functions of the devices and eliminates the need for multicell connection or a voltage promoting circuit and therefore avoiding associated issues. The broader operational time frames (up to 300 h) also enable possible *in vivo* therapeutic functions over a prolonged period. Such a battery system could serve as an essential power tool for sensing and stimulation in the human body or in the environments, and can be fully degradable after usage without unnecessary materials' retention. With an appropriate choice of encapsulation and electrolyte materials, the system can provide stable operational characteristics followed by gradual dissolution at a later stage, i.e., the cell can power an LED in aqueous solution for over 16 h (Figure 3B).

The materials proposed for the degradable battery have been shown to possess desirable biocompatibility. Magnesium, alginate hydrogel, PLGA, and polyanhydride have been applied in many fields of biomaterials (e.g., tissue regeneration, cardiovascular stent, and drug delivery); Mo metal has been investigated for implantable bioresorbable pressure and neural sensor;<sup>[6,7]</sup> and MoO<sub>3</sub> has been reported as an additional component of bioactive xerogels<sup>[46]</sup> or melt-derived glasses,<sup>[37]</sup> which demonstrates desirable *in vitro* bioactivity and biocompatibility. In the current work, the *in vitro* cell viability and subdermal implantation of the full battery show no overt toxicity. These results suggest that by using a proper encapsulation layer and controlling the amount of battery components, the releasing rates of dissolution products can potentially be managed at a safe level.

In this work, we report a high-performance fully biodegradable Mg–MoO<sub>3</sub> battery that consists of all dissolvable materials including Mg, MoO<sub>3</sub>, Mo, sodium alginate hydrogel, PLGA, and polyanhydride encapsulation layer. The battery is capable of providing a high stable output voltage up to 1.6 V as well

as desirable capacity ( $6.5 \text{ mAh cm}^{-2}$ ) and prolonged lifetime up to 13 d. The battery is capable of driving typical ultralow-power implantable electronics with robust functions. Demonstrated operations include a red LED, a calculator, and the amplifier of an ECG signal detector. The battery exhibits desirable biocompatibility and is fully biodegradable both in vivo and in vitro. The battery can potentially be used as an on-board power source to achieve self-powered therapeutic systems for tissue regeneration, presurgery, or postsurgery monitoring over extended periods, which would otherwise be impossible due to the limitations of currently available power tools. The novel materials' strategies and fabrication schemes of the battery system offer a promising approach for advanced power supplies, and provide a critical step along the route to achieve fully functional transient systems that could play an essential role in green electronics, minimizing the environmental impacts and implantable bioresorbable therapeutic and diagnostic systems eliminating secondary surgery for device removal.

## Experimental Section

**Materials and Battery Assembly:** The paste cathode was achieved by mixing powders ( $\text{MoO}_3$  or Mo, Sigma-Aldrich, China) with PLGA (65:35,  $M_w = 75\,000$  Jinan Daigang Biomaterial Co., Ltd, China) polymer dissolved in acetone, with a ratio of powder/PLGA/acetone being 2 g/0.5 g/8 mL. The paste was casted on a molybdenum thin foil ( $30 \mu\text{m}$  for battery discharging and  $5 \mu\text{m}$  for dissolution tests).  $\text{MoO}_3$  thin film of thickness  $\approx 1 \mu\text{m}$  was deposited through a magnetron sputter (100 W, 5 Pa Ar, JGP280, SKY Technology Development Co., Ltd, CAS). Mg foil was used as the anode, with a thickness of  $50 \mu\text{m}$  for in vitro and in vivo degradation evaluation, and  $200 \mu\text{m}$  for discharging and electrochemical tests. Alginate cross-linked by calcium ions was adopted as the electrolyte. It was prepared by dissolving ALG-Na (Sinopharm Chemical Reagent Limited Co., Ltd, China) in the phosphate buffered solution (pH 7.4, with  $0.85 \text{ g L}^{-1} \text{ K}_2\text{HPO}_4$  and  $3.35 \text{ g L}^{-1} \text{ NaH}_2\text{PO}_4$ ), with an ALG-Na concentration of  $0.04 \text{ g mL}^{-1}$ , followed by the addition of 3 mL calcium chloride solution ( $0.1 \text{ g mL}^{-1}$ , Sinopharm Chemical Reagent Co., Ltd, China) to achieve the cross-linking. The dissolution of sodium alginate was accelerated by increasing the temperature to  $70 \text{ }^\circ\text{C}$ . The hydrogel was then shape into a size of  $2 \times 2 \times 0.5 \text{ cm}$  during the cross-linking process which can take up to 6 h. The battery was fabricated by stacking the electrodes and electrolyte layer by layer, with an outermost encapsulation layer of biodegradable UV-curable polyanhydride on top of a thin PLGA layer. The polyanhydride layer was prepared following a previous recipe,<sup>[20]</sup> including mixing the pentaerythritol tetrakis (3-mercaptopropionate), 4-pentenoic anhydride, and poly(ethylene glycol) diacrylate at the molar ratio of 5:7:3 and the addition of a photoinitiator 2,2-dimethoxy-2-phenylacetophenone (0.4%, all from Sigma-Aldrich Corporation, China). The precured polymer was pasted on the surface of the battery and cured under UV light ( $365 \text{ nm}$ ,  $36 \text{ W}$ ) for 30 s.

**Battery Discharge and Electrochemical Testing:** The discharge behavior was performed using a battery tester (Neware Electronic Corporation, Shenzhen, China) as a function of current density and the thickness of the  $\text{MoO}_3$  layer. Long-term evaluation of battery performance was carried out over 300 h with a  $\text{MoO}_3$  thickness of  $200 \mu\text{m}$  at a discharge current density of  $0.025 \text{ mA cm}^{-2}$ . To keep the water content of the hydrogel electrolyte, long-term experiments were performed in humid air (with saturated water vapor pressure at room temperature). Moreover, electrochemical properties of the biodegradable battery were evaluated by a Gamry Potentiostat Reference 600 (Gamry Instruments, Warminster, PA), through galvanostatic and galvanodynamic scanning, EIS, and CV techniques. The two-electrode configuration was used for the full cell testing, and the three-electrode configuration was used for investigating the electrochemical characteristics of the individual

electrode. Saturated silver/silver chloride (Ag/AgCl) was used as the reference electrode.

**Battery Function Demonstration—LED Lighting:** An LED was connected to the biodegradable battery with the assistance of the silver paste and epoxy. The whole battery and the LED were encapsulated with a layer of polyanhydride on top of the PLGA layer and were immersed in a phosphate buffered saline, and the performance was monitored over time.

**Battery Function Demonstration—Powering the Calculator:** The original power source (solar cell) of the calculator was replaced by the proposed single cell Mg– $\text{MoO}_3$  battery, and the functions were evaluated.

**Battery Function Demonstration—ECG Signal Detection:** The battery was connected to a customized low-noise amplifier (LNA) with a power consumption of  $3.24 \mu\text{W}$  under a supply voltage of 1.3 V. An off-the-shelf amplifier, OPA2313, was used as the second stage for the ECG signal acquisition. An over  $\times 100$  amplification was achieved. The output of the second stage was captured by an oscilloscope (form NI PXie-1082).

**Characterization of Materials and Dissolution Behavior:** The morphology of electrode materials was investigated by a field-emission SEM (Zeiss Melin, Germany), and EDS technique was used to analyze the materials' compositions. The dissolution experiments were performed in phosphate buffered saline at  $37$  or  $85 \text{ }^\circ\text{C}$  using a water bath. The solutions were refreshed every day, and optical images were captured at various stages.

**Cell Cytotoxicity and In Vivo Tests—In Vitro Studies:** Cell cytotoxicity was assessed by the CCK-8 assay and Calcein-AM/PI staining. Specifically, L-929 cells (mouse C3H/An subcutaneous connective tissue) acquired from American Type Culture Collection (ATCC) were cultured in RPMI-1640 medium supplemented with 10% fetal bovine serum (FBS) and 1% penicillin/streptomycin. First, PLGA and  $\text{MoO}_3$ -PLGA sterilized by UV light were put into the 24-well plate with a cell density of  $1 \times 10^5$  cells per well, and incubated in 5%  $\text{CO}_2$  at  $37 \text{ }^\circ\text{C}$ . After incubation for 24, 48, and 120 h, the medium was removed and  $100 \mu\text{L}$  of CCK-8 reagents was added to each well to determine the cell viabilities. A microplate reader (Varioskan LUX, Thermo Fisher Scientific Inc., Waltham, MA, USA) was used to measure the optical density (OD) value at a wavelength of 450 nm. Meanwhile, after the CCK-8 reagents were removed, the cells were washed twice with PBS and then stained with Calcein-AM and PI, respectively. The fluorescence images were obtained with fluorescence microscopy (DM IL LED, Leica, Germany). The culture medium was refreshed every day, and the medium at 1, 3, and 5 d was sampled to evaluate the Mo concentration by ICP-OES (Thermo IRIS Intrepid II, China).

**Cell Cytotoxicity and In Vivo Tests—In Vivo Studies:** Animal care was in accordance with the institutional guidelines of Tsinghua University. Protocols were proved by the Institutional Animal Care and Use Committee (IACUC) at Tsinghua University. In vivo experiments were performed through implantation of the encapsulated battery under the skin of the SD rats following a biological evaluation of local reaction after implantation by medical instruments (GB/T 1688.6, China). To demonstrate the biocompatibility and in vivo degradation of the battery, the rats were sacrificed and dissected at the time of 1, 2, and 4 weeks after implantation. The frozen sections of different organs and tissue around the implantation site were subjected to HE staining.

## Supporting Information

Supporting Information is available from the Wiley Online Library or from the author.

## Acknowledgements

This work was supported by National Natural Science Foundation of China (NSFC) 51601103 (L.Y.) and 1000 Youth Talents Program in China (L.Y.).

## Conflict of Interest

The authors declare no conflict of interest.

## Keywords

biodegradable batteries, magnesium, molybdenum trioxide, self-powered electronics, transient electronics

Received: March 14, 2018  
Revised: April 13, 2018  
Published online: May 27, 2018

- [1] S.-W. Hwang, H. Tao, D.-H. Kim, H. Cheng, J.-K. Song, E. Rill, M. A. Brenckle, B. Panilaitis, S. M. Won, Y.-S. Kim, Y. M. Song, K. J. Yu, A. Ameen, R. Li, Y. Su, M. Yang, D. L. Kaplan, M. R. Zakin, M. J. Slepian, Y. Huang, F. G. Omenetto, J. A. Rogers, *Science* **2012**, 337, 1640.
- [2] S.-W. Hwang, G. Park, H. Cheng, J.-K. Song, S.-K. Kang, L. Yin, J.-H. Kim, F. G. Omenetto, Y. Huang, K.-M. Lee, J. A. Rogers, *Adv. Mater.* **2014**, 26, 1992.
- [3] Y. Zhang, B. Lu, H. Xu, X. Feng, *Sci. China: Phys. Mech. Astron.* **2016**, 46, 044605-1.
- [4] K. K. Fu, Z. Wang, J. Dai, M. Carter, L. Hu, *Chem. Mater.* **2016**, 28, 3527.
- [5] R. Li, L. Wang, D. Kong, L. Yin, *Bioact. Mater.* **2018**, 3, 332.
- [6] K. J. Yu, D. Kuzum, S.-W. Hwang, B. H. Kim, H. Juul, N. H. Kim, S. M. Won, K. Chiang, M. Trumpis, A. G. Richardson, H. Cheng, H. Fang, M. Thompson, H. Bink, D. Talos, K. J. Seo, H. N. Lee, S.-K. Kang, J.-H. Kim, J. Y. Lee, Y. Huang, F. E. Jensen, M. A. Dichter, T. H. Lucas, J. Viveni, B. Litt, J. A. Rogers, *Nat. Mater.* **2016**, 15, 782.
- [7] S.-K. Kang, R. K. J. Murphy, S.-W. Hwang, S. M. Lee, D. V. Harburg, N. A. Krueger, J. Shin, P. Gamble, H. Cheng, S. Yu, Z. Liu, J. G. McCall, M. Stephen, H. Ying, J. Kim, G. Park, R. C. Webb, C. H. Lee, S. Chung, D. S. Wie, A. D. Gujar, B. Vemulapalli, A. H. Kim, K.-M. Lee, J. Cheng, Y. Huang, S. H. Lee, P. V. Braun, W. Z. Ray, J. A. Rogers, *Nature* **2016**, 530, 71.
- [8] X. Huang, Y. Liu, S.-W. Hwang, S.-K. Kang, D. Patnaik, J. F. Cortes, J. A. Rogers, *Adv. Mater.* **2014**, 26, 7371.
- [9] C. H. Lee, J.-W. Jeong, Y. Liu, Y. Zhang, Y. Shi, S.-K. Kang, J. Kim, J. S. Kim, N. Y. Lee, B. H. Kim, K.-I. Jang, L. Yin, M. K. Kim, A. Banks, U. Paik, Y. Huang, J. A. Rogers, *Adv. Funct. Mater.* **2015**, 25, 1338.
- [10] Y. K. Lee, K. J. Yu, E. Song, A. B. Farimani, F. Vitale, Z. Xie, Y. Yoon, Y. Kim, A. Richardson, H. Luan, Y. Wu, X. Xie, T. H. Lucas, K. Crawford, Y. Mei, X. Feng, Y. Huang, B. Litt, N. R. Aluru, L. Yin, J. A. Rogers, *ACS Nano* **2017**, 11, 12562.
- [11] Y. Gao, Y. Zhang, X. Wang, K. Sim, J. Liu, J. Chen, X. Feng, H. Xu, C. Yu, *Sci. Adv.* **2017**, 3, e1701222.
- [12] S.-W. Hwang, X. Huang, J.-H. Seo, J.-K. Song, S. Kim, S. Hage-Ali, H.-J. Chung, H. Tao, F. G. Omenetto, Z. Ma, J. A. Rogers, *Adv. Mater.* **2013**, 25, 3526.
- [13] C. Dagdeviren, S.-W. Hwang, Y. Su, S. Kim, H. Cheng, O. Gur, R. Haney, F. G. Omenetto, Y. Huang, J. A. Rogers, *Small* **2013**, 9, 3398.
- [14] X. Wang, W. Xu, P. Chatterjee, C. Lv, J. Popovich, Z. Song, L. Dai, M. Y. S. Kalani, S. E. Haydel, H. Jiang, *Adv. Mater. Technol.* **2016**, 1, 1600059.
- [15] G. Lee, S.-K. Kang, S. M. Won, P. Gutruf, Y. R. Jeong, J. Koo, S.-S. Lee, J. A. Rogers, J. S. Ha, *Adv. Energy Mater.* **2017**, 7, 1700157.
- [16] L. Lu, Z. Yang, K. Meacham, C. Cvetkovic, A. Corbin Elise, A. Vázquez-Guardado, M. Xue, L. Yin, J. Boroumand, G. Pakeltis, T. Sang, J. Yu Ki, D. Chanda, R. Bashir, W. Gereau Robert, X. Sheng, A. Rogers John, *Adv. Energy Mater.* **2018**, 8, 1703035.
- [17] B. Scrosati, J. Garche, *J. Power Sources* **2010**, 195, 2419.
- [18] L. Yin, H. Cheng, S. Mao, R. Haasch, Y. Liu, X. Xie, S.-W. Hwang, H. Jain, S.-K. Kang, Y. Su, R. Li, Y. Huang, J. A. Rogers, *Adv. Funct. Mater.* **2014**, 24, 645.
- [19] G. E. Luckachan, C. K. S. Pillai, *J. Polym. Environ.* **2011**, 19, 637.
- [20] L. Yin, X. Huang, H. Xu, Y. Zhang, J. Lam, J. Cheng, J. A. Rogers, *Adv. Mater.* **2014**, 26, 3879.
- [21] P. Nadeau, D. El-Damak, D. Glettig, Y. L. Kong, S. Mo, C. Cleveland, L. Booth, N. Roxhed, R. Langer, A. P. Chandrakasan, G. Traverso, *Nat. Biomed. Eng.* **2017**, 1, 0022.
- [22] H. Hafezi, T. L. Robertson, G. D. Moon, K. Y. Au-Yeung, M. J. Zdeblick, G. M. Savage, *IEEE Trans. Biomed. Eng.* **2015**, 62, 99.
- [23] M. Tsang, A. Armutlulu, A. W. Martinez, S. A. B. Allen, M. G. Allen, *Microsyst. Nanoeng.* **2015**, 1, 15024.
- [24] M. Tsang, A. Armutlulu, A. Martinez, F. Herrault, S. A. B. Allen, M. G. Allen, in *2014 IEEE 27th Int. Conf. on Micro Electro Mechanical Systems (MEMS)*, IEEE, Piscataway, NJ **2014**, p. 358.
- [25] X. Jia, Y. Yang, C. Wang, C. Zhao, R. Vijayaraghavan, D. R. MacFarlane, M. Forsyth, G. G. Wallace, *ACS Appl. Mater. Interfaces* **2014**, 6, 21110.
- [26] X. Jia, C. Wang, C. Zhao, Y. Ge, G. G. Wallace, *Adv. Funct. Mater.* **2016**, 26, 1454.
- [27] X. Jia, C. Wang, V. Ranganathan, B. Napier, C. Yu, Y. Chao, M. Forsyth, F. G. Omenetto, D. R. MacFarlane, G. G. Wallace, *ACS Energy Lett.* **2017**, 2, 831.
- [28] Y. J. Kim, W. Wu, S.-E. Chun, J. F. Whitacre, C. J. Bettinger, *Proc. Natl. Acad. Sci. USA* **2013**, 110, 20912.
- [29] Y. J. Kim, S.-E. Chun, J. Whitacre, C. J. Bettinger, *J. Mater. Chem. B* **2013**, 1, 3781.
- [30] Z. Zhu, T. Kin Tam, F. Sun, C. You, Y. H. Percival Zhang, *Nat. Commun.* **2014**, 5, 3026.
- [31] A. Heller, *Phys. Chem. Chem. Phys.* **2004**, 6, 209.
- [32] K. Fu, Z. Liu, Y. Yao, Z. Wang, B. Zhao, W. Luo, J. Dai, S. D. Lacey, L. Zhou, F. Shen, M. Kim, L. Swafford, L. Sengupta, L. Hu, *Nano Lett.* **2015**, 15, 4664.
- [33] Y. Chen, R. Jamshidi, K. White, S. Çinar, E. Gallegos, N. Hashemi, R. Montazami, *J. Polym. Sci., Part B: Polym. Phys.* **2016**, 54, 2021.
- [34] J. P. Esquivel, P. Alday, O. A. Ibrahim, B. Fernández, E. Kjeang, N. Sabaté, *Adv. Energy Mater.* **2017**, 7, 1700275.
- [35] I. A. de Castro, R. S. Datta, J. Z. Ou, A. Castellanos-Gomez, S. Sriram, T. Daeneke, K. Kalantar-zadeh, *Adv. Mater.* **2017**, 29, 31.
- [36] Institute of Medicine, in *Dietary Reference Intakes for Vitamin A, Vitamin K, Arsenic, Boron, Chromium, Copper, Iodine, Iron, Manganese, Molybdenum, Nickel, Silicon, Vanadium, and Zinc*, The National Academies Press, Washington, DC **2001**, p. 800.
- [37] R. C. Lucacel, O. Ponta, E. Licarete, T. Radu, V. Simon, *J. Non-Cryst. Solids* **2016**, 439, 67.
- [38] M. E. Sinangil, M. Yip, M. Qazi, R. Rithe, J. Kwong, A. P. Chandrakasan, *IEEE Trans. Circuits Syst. II: Express Briefs* **2012**, 59, 533.
- [39] A. Demosthenous, *Adv. Electron.* **2014**, 2014, 21.
- [40] A. Amar, A. Kouki, H. Cao, *Sensors* **2015**, 15, 28889.
- [41] S. K. Kang, S. W. Hwang, S. Yu, J. H. Seo, E. A. Corbin, J. Shin, D. S. Wie, R. Bashir, Z. Q. Ma, J. A. Rogers, *Adv. Funct. Mater.* **2015**, 25, 1789.
- [42] D. N. Kapoor, A. Bhatia, R. Kaur, R. Sharma, G. Kaur, S. Dhawan, *Ther. Delivery* **2015**, 6, 41.
- [43] E. Vey, C. Rodger, J. Booth, M. Claybourn, A. F. Miller, A. Saiani, *Polym. Degrad. Stab.* **2011**, 96, 1882.
- [44] A. Göpferich, J. Tessmar, *Adv. Drug Delivery Rev.* **2002**, 54, 911.
- [45] G.ershinsky, H. D. Yoo, Y. Gofer, D. Aurbach, *Langmuir* **2013**, 29, 10964.
- [46] O. Ponta, R. Ciceo-Lucacel, A. Vulpoi, T. Radu, S. Simon, *J. Biomed. Mater. Res. A* **2014**, 102, 3177.